A Deep Learning Framework for Analysis of the Eustachian Tube and the Internal Carotid Artery

Ameen Amanian, MD, MSE[1,2,3] (iD), Aseem Jain, MSE[1,4] (iD),
Yuliang Xiao, MSE[5], Chanha Kim, BS[5],
Andy S. Ding, MD, MSE[2], Manish Sahu, PhD[5],
Russell Taylor, PhD[5], Mathias Unberath, PhD[5],
Bryan K. Ward, MD[2], Deepa Galaiya, MD[2],
Masaru Ishii, MD PhD[2], and Francis X. Creighton, MD[2]

Abstract

Objective. Obtaining automated, objective 3-dimensional (3D) models of the Eustachian tube (ET) and the internal carotid artery (ICA) from computed tomography (CT) scans could provide useful navigational and diagnostic information for ET pathologies and interventions. We aim to develop a deep learning (DL) pipeline to automatically segment the ET and ICA and use these segmentations to compute distances between these structures.

Study Design. Retrospective cohort.

Setting. Tertiary referral center.

Methods. From a database of 30 CT scans, 60 ET and ICA pairs were manually segmented and used to train an nnU-Net model, a DL segmentation framework. These segmentations were also used to develop a quantitative tool to capture the magnitude and location of the minimum distance point (MDP) between ET and ICA. Performance metrics for the nnU-Net automated segmentations were calculated via the average Hausdorff distance (AHD) and dice similarity coefficient (DSC).

Results. The AHD for the ET and ICA were 0.922 and 0.246 mm, respectively. Similarly, the DSC values for the ET and ICA were 0.578 and 0.884. The mean MDP from ET to ICA in the cartilaginous region was 2.6 mm (0.7-5.3 mm) and was located on average 1.9 mm caudal from the bony cartilaginous junction.

Conclusion. This study describes the first end-to-end DL pipeline for automated ET and ICA segmentation and analyzes distances between these structures. In addition to helping to ensure the safe selection of patients for ET dilation, this method can facilitate large-scale studies exploring the relationship between ET pathologies and the 3D shape of the ET.

Keywords

artificial intelligence, deep learning, Eustachian tube, Eustachian tube balloon dilation, Eustachian tube dysfunction, medical imaging

Obstructive Eustachian tube dysfunction (ETD) is characterized by a wide spectrum of symptoms, including ear fullness, pressure, pain, and hearing loss, among others, due to an inability of the middle ear to regulate pressure adequately.[1] Current research estimates the prevalence of ETD to be around 1% to 2% of the population, with some studies reporting rates as high as 4.6%.[2,3] Despite its prevalence, the diagnosis and management of obstructive ETD have significant room for improvement under the current standard of care.[4] For instance, in otitis media with effusion, which is likely related to obstructive ETD, the use of medical therapies including nasal steroids, antihistamines, antibiotics, and so forth, remains ineffective.[4]

Due to the lack of robust, objective data obtained from current diagnostic tools for ETD, clinicians have turned toward imaging such as computed tomography (CT) or magnetic resonance imaging (MRI) to understand better the Eustachian tube's (ET's) structure along its cartilaginous and osseous components.[5-8] However, most radiographic morphology measurements have been done from a 2-dimensional (2D) perspective, and due to the complex

[1]Department of Biomedical Engineering, Whiting School of Engineering, Johns Hopkins University, Baltimore, Maryland, USA
[2]Department of Otolaryngology–Head and Neck Surgery, Johns Hopkins University School of Medicine, Baltimore, Maryland, USA
[3]Department of Otolaryngology–Head and Neck Surgery, University of British Colombia, Vancouver, British Colombia, Canada
[4]Department of Otolaryngology–Head and Neck Surgery, University of Cincinnati, Cincinnati, Ohio, USA
[5]Department of Computer Science, Johns Hopkins University, Baltimore, Maryland, USA

Corresponding Author:
Ameen Amanian, MD, MSE, Division of Otolaryngology–Head and Neck Surgery, Department of Surgery, University of British Columbia, 4th floor, Gordon and Leslie Diamond Health Care Center, 2775 Laurel Street, Vancouver, BC V5Z1M9, Canada.
Email: ma.amanian@alumni.ubc.ca

3-dimensional (3D) structure of the ET, these results have been difficult to translate into the clinical domain.[7] Creating a 3D rendition of the ET would allow clinicians to study the intricate anatomy of this structure further and pave the path for correlating certain parts of the tube (eg, pharyngeal orifice) to patient-reported symptoms and nearby anatomical structures.

Generating 3D models of the ET and nearby critical structures may also improve the understanding and management of ETD. Since Food and Drug Administration approval in 2016, Eustachian tube balloon dilation (ETBD) has become a common operative treatment of ETD.[9,10] Although rare, one of the most feared complications of the ETBD is damage to critical structures, including the internal carotid artery (ICA).[11,12] Given the potential severity, understanding the distance between the ICA and ET (dICA) remains crucial in the preoperative evaluation of patients undergoing ETBD. To assess for dICA, patients typically receive a temporal bone CT scan before ETBD.[13] Prior groups have quantified dICA from such scans by manually measuring distances at various points along the ET.[2,14] However, the manual measurement of this task is time-consuming and prone to interreader variability.[15] Further, this task is typically done along 2D slices, which can misrepresent the true spatial distance between the ET and ICA. Creating accurate 3D representations of the ET and ICA and automatically calculating the distance between these structures would augment the preoperative evaluation and could further decrease the risk of injury to the ICA during ETBD.

Despite the advantages of 3D analysis, manual construction of the 3D models of the ET and ICA is a time-consuming, technically difficult task and difficult to apply to large population datasets. However, recent advances in deep learning (DL) enable researchers to automatically segment structures from CT scans to create accurate 3D models.[16] Our group has previously successfully developed autonomous pipelines for automatically segmenting structures of the temporal bone.[17] In this study, we aim to build on this prior work to develop a DL pipeline to (1) automatically segment the ET and ICA and generate accurate 3D models from CT scans and (2) extend this pipeline to automatically extract the minimum dICA from these 3D models. We hope this can serve as the foundation to allow our field to harness large-scale radiographic datasets to understand ET anatomy better and use radiographic assessments to aid in the future diagnosis and management of ET pathologies.

Methods

Figure 1 summarizes the proposed end-to-end pipeline to segment the ET and ICA from CT scans using DL and to analyze the minimum distance between the ET and the ICA from the segmentations.

Ethics

This study was approved by the Institutional Review Board at Johns Hopkins School of Medicine. Prior to manual annotation of the high-resolution CT images, they were deidentified and defaced by removal of the soft tissue structures of the face.

Ground Truth Segmentation Dataset

This study used an anonymized dataset of 30 head and neck CT scans without contrast of patients with no apparent craniofacial abnormalities to assess 60 ETs. The resolution of the axial cuts of the CT scans was 512×512 pixels with a slice thickness of 0.4 mm. Each scan was manually segmented by an otolaryngologist (A.A.) and used to generate 3D models of the ET and the ICA in 3D Slicer®.[18] The bony and nasopharyngeal portions of the ET were labeled by segmenting the air-soft tissue gap in both locations, respectively. For the cartilaginous portion, the lumen of ET may be difficult to discern; to resolve this, the annotator applied a local histogram to better discern the lumen from the soft tissue of the surrounding structures. The ET models were subdivided into 2 regions: the bony portion (within the temporal bone) of the ET and the cartilaginous region. The bony portion of the ET tube was defined as beginning at the tympanic ostium and ending at the isthmus, the narrowest point along the ET (referred to as the bony cartilaginous [BC] junction in this paper). The cartilaginous region was defined from the BC junction to the opening of the nasopharynx. The ICA was segmented from the petrous
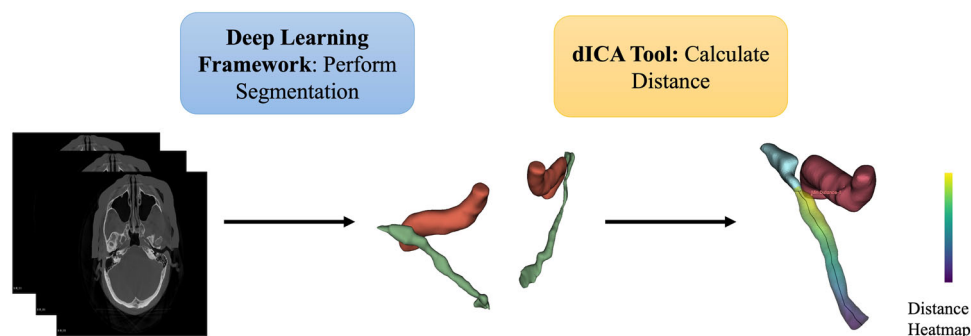

Figure 1. Overview of the method to (1) segment ET and ICA and (2) compute the distance heatmap between them. dICA, distance between the ICA and ET; ET, Eustachian tube; ICA, internal carotid artery.

segment to the vertical portion for each scan. An additional rater (A.J.) manually segmented the ET across the 30 scans to further support the accuracy of the ET segmentations. ICA segmentations were not repeated as these are well defined structures with well-defined bony borders on CT scans. A senior otolaryngologists (F.X.C.) reviewed and revised the segmentations if any significant discrepancies were identified among the 2 raters.

Interrater Segmentation Comparison

Multiple metrics were used to compute differences between raters' segmentations including average Hausdorff distance (AHD), dice similarity coefficient (DSC), and Cohen κ coefficient. AHD was calculated to measure the distance in mm between 2 pointsets (ie, rater 1 and rater 2).[19] For this, the closest distance between each point on both raters' segmentation is determined, and the average of the distances is calculated to result in the AHD achieving submillimeter accuracy. The DSC was calculated as the secondary outcome, determining the volumetric overlap between the 2 raters.[20] A score of 1 correlates with perfect overlap, whereas 0 indicates no overlap.[20] In addition to AHD and DCS, Cohen κ coefficient is often used to computer interrater agreements in medical image segmentations.[21] It is represented by the formula below, where TP = true positive, TN = true negative, FP = false positive, and FN = false negative. In general, k scores above 0.4 are in moderate agreement or better

$$k = 2 \times \frac{\text{TP} \times \text{TN} - \text{FN} \times \text{FP}}{(\text{TP} + \text{FP}) \times (\text{FP} + \text{TN}) + (\text{TP} + \text{FN}) \times (\text{FN} + \text{TN})}.$$

DL Framework

Before creating the DL segmentation network, we ensured the CT scans were co-aligned using the Advanced Normalization Tools software.[22] To train the segmentation network, we used nnU-Net, a supervised DL framework providing state-of-the-art image segmentation within the medical domain.[16] The co-aligned scans and corresponding segmentations were passed through the nnU-Net DL. Five-fold cross-validation with 100 epochs per fold was utilized to train the final model. In each fold, the dataset was assigned to a training and testing set in a 0.7:0.3 fashion (25 training scans, 5 test scans). Via this configuration, each image would be assigned to a testing set in at least one of the folds to account for overfitting. Upon completion of training, the framework selected the best model based on its validation performance. Predictions (ie, inference) were then provided on the test images, unseen by the model during training.

To quantify the performance of our DL framework, we utilized multiple measurement tools to compare the predictions' accuracy to the ground truths created by A.A. and A.J. Ground truths created by A.J. were not used during the training process. For our primary and

secondary outcome, the AHD and DSC were similarly utilized as highlighted above in 'Inter-Rater Segmentation Comparison'.

dICA Tool

After the automated generation of the 3D models of the ET and ICA, the models were analyzed using the dICA tool to extract the magnitude and location of the minimum distance point (MDP). The proposed tool was built using Python and existing packages within 3D Slicer.[18] As shown in **Figure 2**, using the Model-to-Model Distance subpackage in 3D Slicer, a distance heat map was automatically generated, in which brighter colors corresponded to decreased distance between the 2 models. This heat map was further analyzed to determine the magnitude of this minimum distance and its location on the surface ET mesh (point labeled in **Figure 2**). The model-to-model distance subpackage calculates the Euclidean distance between 2 mesh point clouds and has been validated in prior papers.[23] The magnitude of the minimum distance was also manually calculated to verify the accuracy of the automated tool.

To determine the location of the MDP, a center line (shown in **Figure 1**) through the ET was computed using the Vascular Modeling Tool Kit subpackage in 3D Slicer.[24] Once the center line was computed through the lumen of the ET, the MDP was projected onto this line to compute the location of the MDP along the center line. The magnitude and location of the MDP were calculated for the 60 ETs in the dataset used for the DL framework.
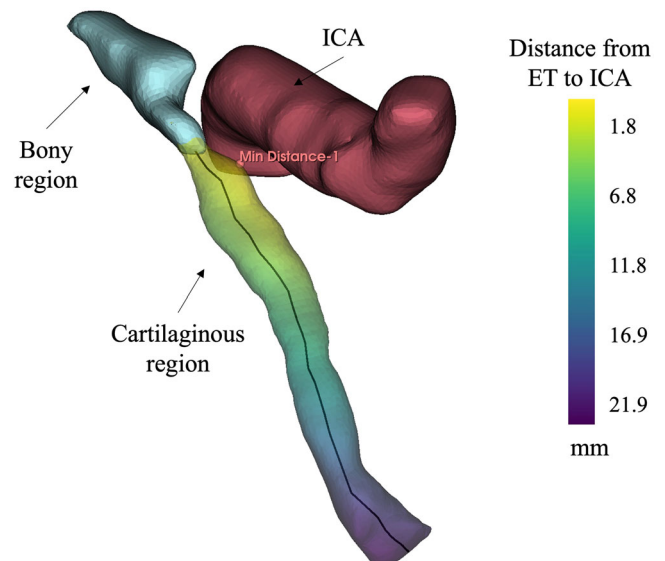

Figure 2. A 3D mesh model of ET with a centerline created through the cartilaginous segment. The calculated minimum distance between the cartilaginous region and ICA is shown with labeled point mid-distance—1. Bony segment and ICA are also shown. 3D, three dimensional; ET, Eustachian tube; ICA, internal carotid artery.

Analysis of dICA Along ET

The proposed dICA tool was also expanded to analyze the MDP's magnitude along the entire ET course. Such analysis would be useful to understand how the distance from the ET to the ICA changes as a balloon catheter is advanced along the ET during ETBD. To simulate a balloon catheter, a sphere with a radius of 2.5 mm (balloon catheters typically have a diameter of 3-6 mm) with center points derived from the centerline was created within the software. The intersection of this sphere with the ET model generated a range of surface points on the heat map shown in **Figure 2**. The average distance from the ET to ICA was computed from this set of points. This process was programmatically repeated for all the points along the centerline for each ET. The time to extract the location and magnitude of the MDP ranged in the order of milliseconds. This data was further analyzed using Matlab®.

Results

The performance metrics assessed via the DL pipeline can be visualized in **Figure 3A** and **B**. Models generated by the DL pipeline were primarily compared against the ground truths created by AA. All segmented structures achieved submillimeter AHD: ET 0.922 ± 0.128 mm and ICA 0.284 ± 0.026 mm. For our secondary outcome, ICA and ET had an average DSC of 0.892 ± 0.052 and 0.575 ± 0.140, respectively. The model achieved similar performance when compared against rater A.J.'s ET

segmentations: AHD of 0.881 ± 0.105 mm and DSC of 0.59 ± 0.116. The total training time using the 5-fold method described above for the nnUnet was around 450 minutes using an RTX 3090 GPU. The inference portion took, on average, 47 seconds per scan for 23.5 minutes for all test images.

As mentioned above, the dICA tool outlined above captured the MDP's magnitude and its location along the ET. As shown in **Figure 4**, the mean magnitude of the MDP along the cartilaginous region was 2.6 mm (standard deviation 0.9 mm, range 0.7-5.3 mm) and 1.0 mm within the bony region (standard deviation 0.5 mm, range 0.1-2 mm). The difference between the bony and the cartilaginous region was statistically significant ($P < .001$). On average (n = 60), the MDP occurred approximately 1.9 mm caudal from the BC junction (standard deviation 2.1 mm, range 0-7.6 mm).

Analysis of the dICA magnitude along the course of the ET beginning from the BC junction is shown in **Figure 5**. The data was subdivided into 2 mm regions (**Table 1**). The covered region ranged from the BC junction to the 20 mm caudal of this junction, as most pathology occurs within this region.[10] A fifth-degree polynomial was fit using the raw data to explore how distance to the ICA changes throughout the course of the ET, starting from the BC junction toward the nasopharyngeal opening. We observed that the distance to the ICA increased (slope of orange curve > 0) around 1.9 mm from the BC junction.
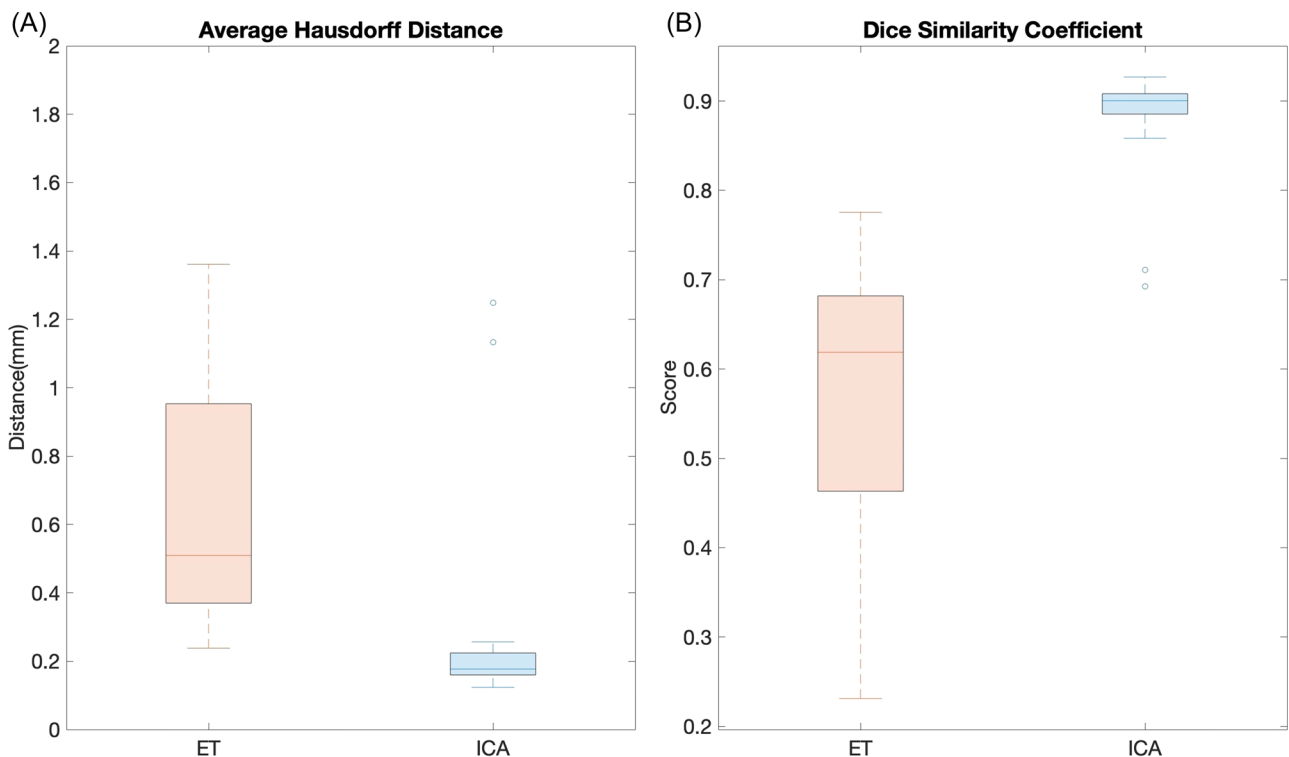

Figure 3. (A) Average Hausdorff distances between the "Ground Truth" segmentations and "Predicted" segmentations for ET and ICA. (B) Dice similarity coefficients between the "Ground Truth" segmentations and "Predicted" segmentations for ET and ICA. ET, Eustachian tube; ICA, internal carotid artery.
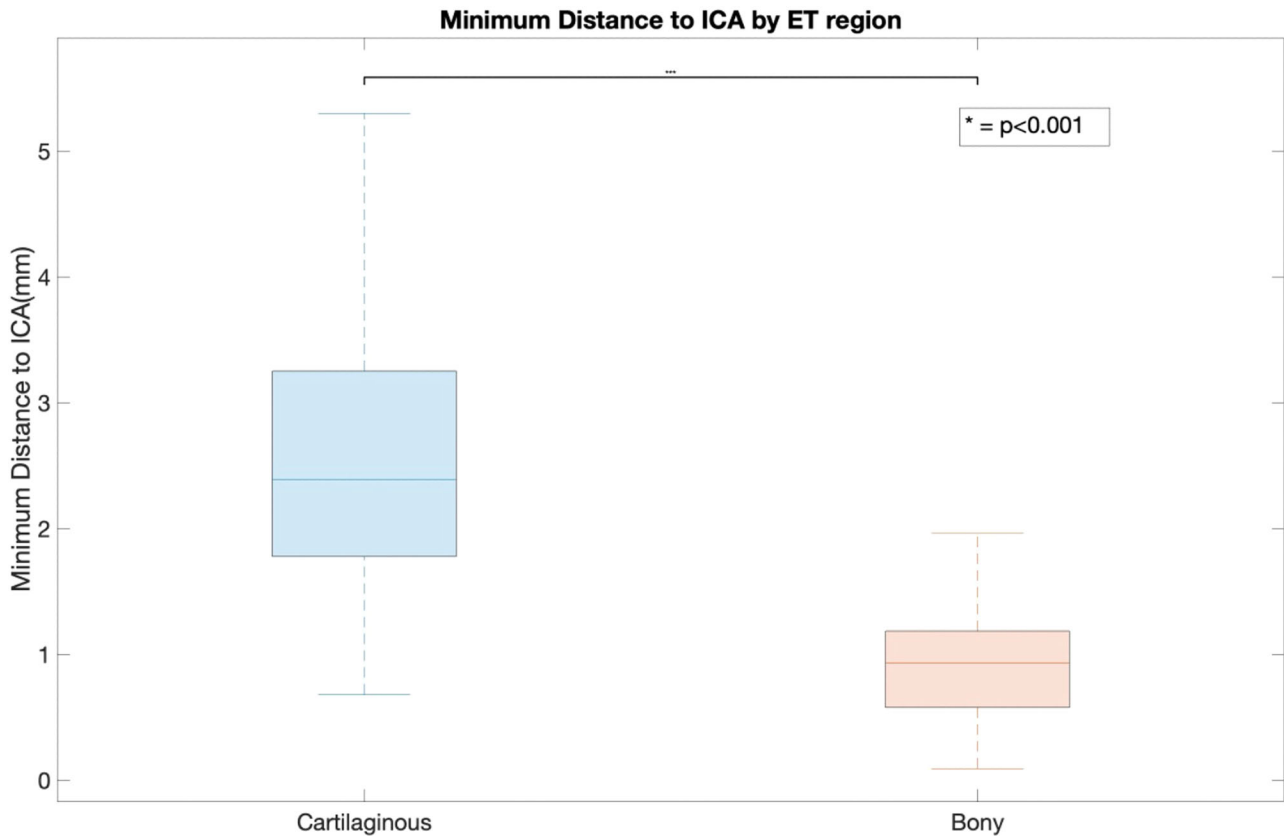
Figure 4. Box and whisker plot of minimum distance to ICA by ET region. ET, Eustachian tube; ICA, internal carotid artery.

Additionally, the minimum distance was manually calculated and compared to the distance generated from the tool, as shown in **Figure 6**, to assess accuracy. There was no statistical difference between manual calculations and those generated by the dICA tool ($P = .24$).

As mentioned above, to further validate the accuracy of the ground truth labels, a second rater annotated the dataset; these ratings were compared to the original dataset using AHD, DSC, and κ scores. In our analysis, the AHD between the raters was equal to 0.51 mm and the DSC score between the 2 raters was 0.65. The average k score was equal to 0.61, and we found k to be less than 0.4 for only 1 scan.

Discussion

ETD is a complex medical condition with no established set of diagnostic tools for management. While the ET is a dynamic structure, a better understanding of its 3D radiographic anatomy could allow for the development of future imaging-based criteria to help augment existing assessment methods for diagnosing and managing ETD. The proposed pipeline outlines an automated method for segmenting and creating 3D models of the ET and ICA from CT scans. We propose a clinically relevant extension, extracting the distance between ICA and the ET for ETBD preoperative assessment. While this pipeline alone

is not sufficient to be used in diagnosing ET pathologies, the creation and validation of this method is a first step in developing large population data sets to understand better the static geometric characteristics of normal and pathologic ET, as well as differences among different age and ethnic groups.

Beyond ETBD preoperative assessment, this pipeline has numerous potential clinical implications. Recently, groups have started testing CT-guided balloon catheter navigation systems for ETBD to avoid injury to ICA.[25] Integrating this tool into such systems could facilitate rapid distance assessment to the MDP as the surgeon advances the balloon catheter. Additionally, automatically creating 3D models of the ET and ICA and analyzing distances between them could facilitate large-scale radiomics studies, which play a role in understanding how various pathologies impact the shape and spatial relationships between these structures. This tool's function can also be expanded to assess other clinically relevant structures segmented from CT scans.

We assessed this DL nnU-Net's accuracy via the AHD and DSC. The AHD metric is more robust and reliable for thin structures (ie, ET), whereas the DSC metric is more prone to variability for small and/or thin structures.[17,19,20,26] As a result, we placed a larger emphasis on the AHD metric as this would better capture the performance for our segmented structures. For the AHD, we achieved submillimeter accuracy with
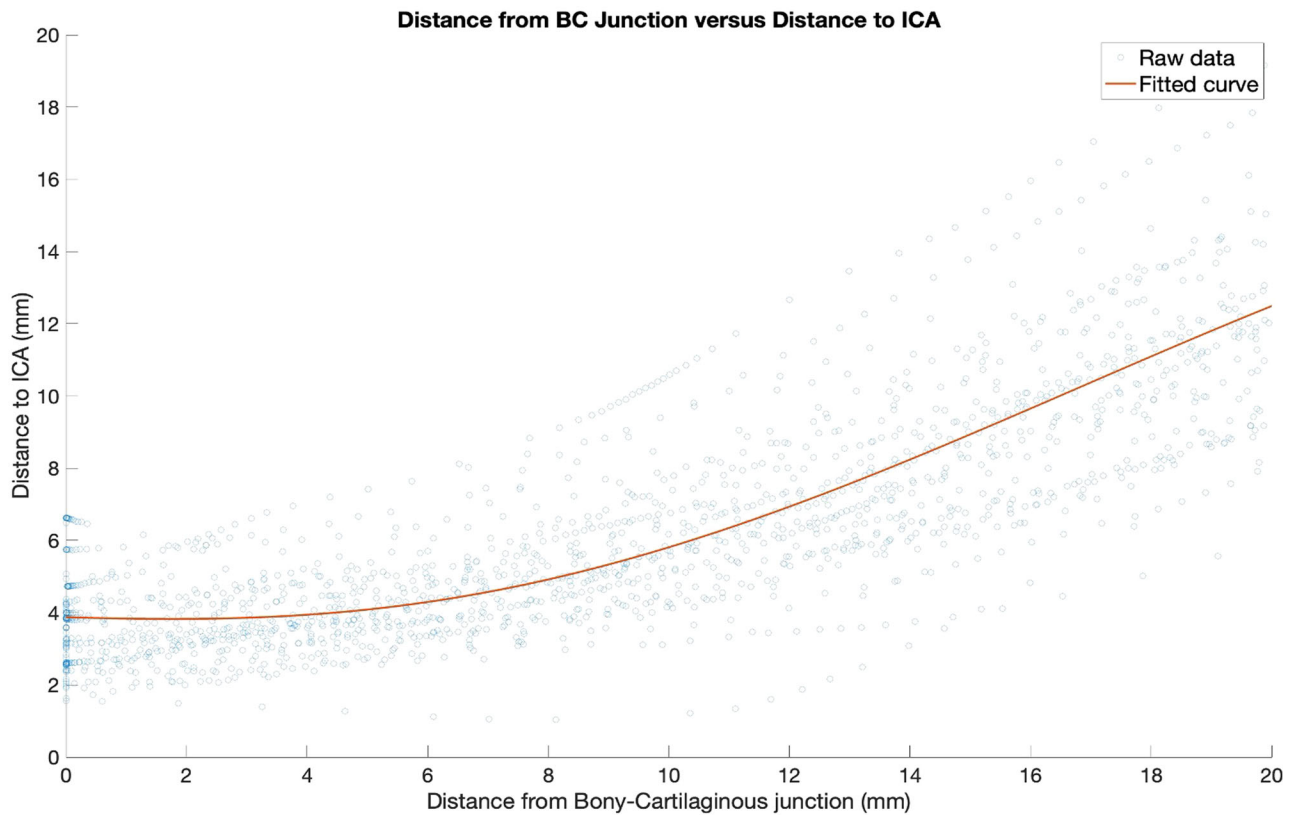
Figure 5. Distance from BC junction versus distance to ICA; dots represent the average distance to ICA along an individual ET at a given distance from the BC joint. The line is a fitted fifth-order polynomial curve generated from dots. BC, bony cartilage; ET, Eustachian tube; ICA, internal carotid artery.

Table 1. Distance to ICA Along the ET

Distance from BC junction (mm)	Average distance to ICA (mm)	Standard deviation of distance to ICA (mm)	Range of distance to ICA (mm)
0-2	3.9	1.28	1.5-6.6
2-4	3.9	1.1	1.4-6.9
4-6	4.1	1.0	1.3-7.0
6-8	4.7	1.2	1.1-8.3
8-10	5.8	2.1	1.2-11.7
10-12	6.6	2.3	1.8-13.9
12-14	7.3	2.5	3.5-15.5
14-16	8.5	2.5	4.4-17.1
16-18	10.3	2.5	5.5-19.2
18-20	11.2	2.5	6.3-20.0

Abbreviations: BC, bony cartilaginous; ET, Eustachian tube; ICA, internal carotid artery.

the ET (AHD 0.992 mm) and the ICA (AHD 0.246 mm). Furthermore, the average DSC score for the ICA was 0.882, demonstrating high accuracy with this structure. Generally, a DSC score of 0.7 and above corresponds to successful radiographic overlap.[20] Although the DSC for the ET was below this threshold (0.575), this was primarily due to the thin nature of the ET structure.

Previous experiments have confirmed that the smaller the structure of interest, the lower the DSC score.[27] In our study, the loss in the DSC coefficient was primarily attributed to the mid-cartilaginous segment of the ET. The thickness of the mid-cartilaginous segment was at times 1 to 3 voxels during annotation, and even a small discrepancy between the ground truth and prediction would result in a significant penalty when calculating this metric.

As mentioned above, prior groups have manually explored minimum dICA, given its importance in preoperative planning, which can be time-consuming and subject to poor interrater reliability.[2,14,28] Olander et al. measured distances between the ICA and ET along 3 separate points: the BC junction, the mid-cartilaginous ET point, and the nasopharyngeal orifice. They found the minimum distance to be 4.2, 24.5, and 61.9 mm, respectively.[2] The minimum distance reported in **Figure 3**, while in the range of this work, is slightly smaller. This can be attributed to 2 factors: (1) the proposed tool measured surface-to-surface distances, whereas Olander et al measured from the ET lumen to the ICA, and (2) as shown in **Figure 5**, while the distance to ICA generally decreases closer to the BC junction, the location of the minimum distance occurs approximately 1.9 mm away from the BC junction rather than at the junction. Additionally, Olander et al acknowledge that an assumption in their study was that minimum distance lies
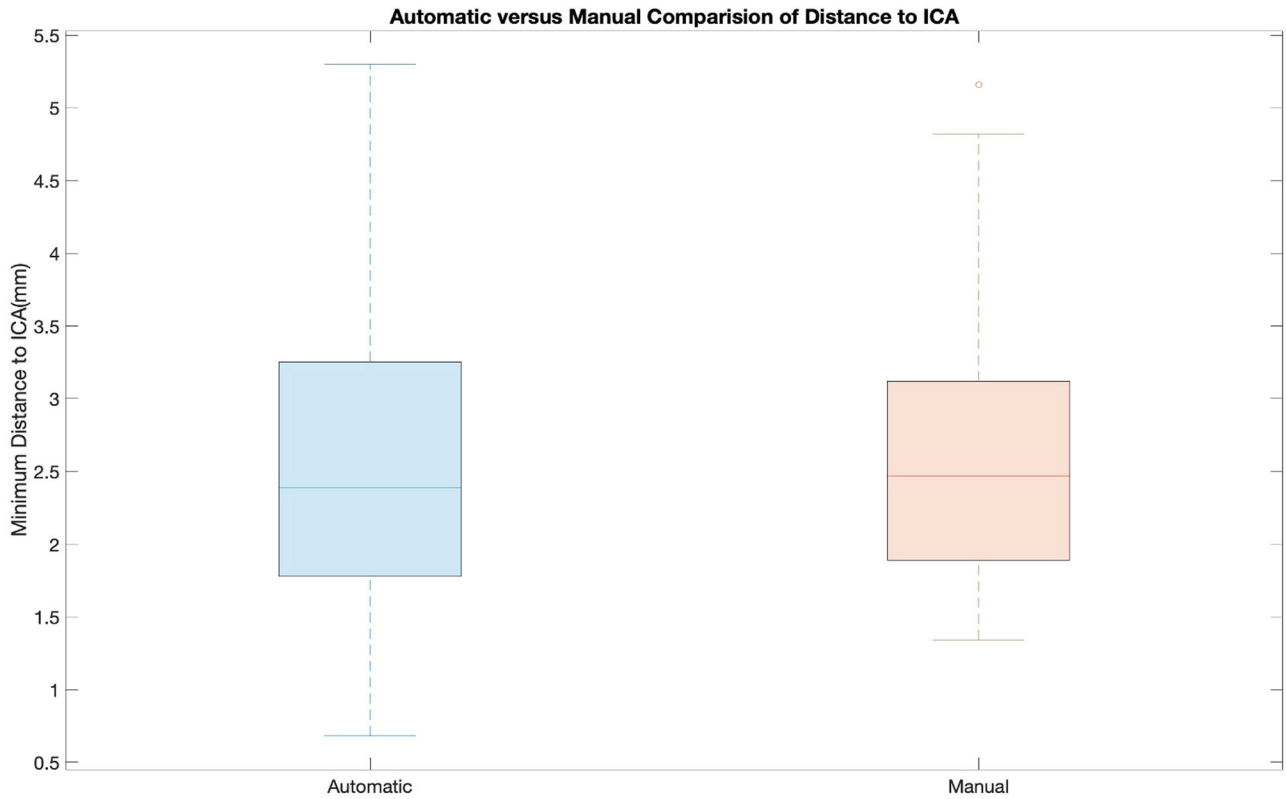
Figure 6. Automatic extraction of distance from ET to ICA compared to manual measurement from ET to ICA. ET, Eustachian tube; ICA, internal carotid artery.

along a 2D plane, even though the ET is angulated.[2] By using 3D mesh files to study spatial geometries, the proposed tool does not have this limitation.

There are several limitations present within the context of this study. First, the image volumes were supine, noncontrast CT images of the head and did not include a Valsalva maneuver for enhanced visualization of the ET. As a result, manual annotation along the middle aspect of the ET was difficult to decipher, which may have led to an inaccurate ground truth along that segment. However, having high κ scores when comparing with a second rater and a senior otolaryngologists verify annotations supports the accuracy of the segmentations. Future studies could use other imaging modalities, such as MRI, that are more sensitive to soft tissue. Second, to train and implement the DL framework, we required access to a workstation with specific computational requirements that may not be available at all centers. Using computationally efficient DL algorithms in the future could reduce the barrier required to implement such models.

Conclusion

To the authors' knowledge, this study describes the first end-to-end DL pipeline for (1) automated ET and ICA segmentation and (2) analysis of distances between these structures. As such, this pipeline can be applied to safely select patients for ETBD and future radiographic assessments focused on improving our anatomical and clinical understanding of the ET. Future work will be targeted at improving the pipeline's accuracy and understanding spatial relations between other relevant structures.

Author Contributions

Ameen Amanian, project conception, data acquisition, and analysis, drafting of the manuscript with revisions and approval of the final manuscript; **Aseem Jain**, data acquisition and analysis, drafting of the manuscript with revisions and approval of final manuscript; **Yuliang Xiao**, data acquisition and analysis, drafting of the manuscript with revisions and approval of the final manuscript; **Chanha Kim**, data acquisition and analysis, drafting of the manuscript with revisions and approval of the final manuscript; **Andy S. Ding**, study conception and design, revision, and final approval of the manuscript; **Manish Sahu**, study conception and design, revision, and final approval of the manuscript; **Russell Taylor**, study conception and design, revision, and final approval of the manuscript; **Mathias Unberath**, study conception and design, revision, and final approval of the manuscript; **Bryan K. Ward**, study conception and design, revision, and final approval of the manuscript; **Deepa Galaiya**, study conception and design, revision, and final approval of the manuscript; **Masaru Ishii**, study conception and design, revision, and final approval of the manuscript; **Francis X. Creighton**, project conception, drafting of the manuscript with revisions and approval of the final manuscript.

Disclosures

ORCID iD

Ameen Amanian ⓘ https://orcid.org/0000-0002-4418-8215
Aseem Jain ⓘ https://orcid.org/0000-0003-2105-4940

References

1. Froehlich MH, Le PT, Nguyen SA, McRackan TR, Rizk HG, Meyer TA. Eustachian tube balloon dilation: a systematic review and meta-analysis of treatment outcomes. *Otolaryngol Head Neck Surg.* 2020;163(5):870-882. doi:10.1177/01945998 20924322

2. Olander H, Järnstedt J, Poe D, Kivekäs I. Critical distance between the cartilaginous Eustachian tube and the internal carotid artery. *Eur Arch Otrhinolaryngol.* 2017;274(1):73-77. doi:10.1007/s00405-016-4187-y

3. Shan A, Ward BK, Goman AM, et al. Prevalence of Eustachian tube dysfunction in adults in the United States. *JAMA Otolaryngol Head Neck Surg.* 2019;145(10):974. doi:10. 1001/jamaoto.2019.1917

4. Rosenfeld RM, Shin JJ, Schwartz SR, et al. Clinical practice guideline: otitis media with effusion (update). *Otolaryngol Head Neck Surg.* 2016;154(1 suppl):S1-S41. doi:10.1177/ 0194599815623467

5. Tucci DL, McCoul ED, Rosenfeld RM, et al. Clinical consensus statement: balloon dilation of the Eustachian tube. *Otolaryngol Head Neck Surg.* 2019;161(1):6-17.

6. McCoul ED, Anand VK, Christos PJ. Validating the clinical assessment of Eustachian tube dysfunction: the Eustachian Tube Dysfunction Questionnaire (ETDQ-7). *Laryngoscope.* 2012;122(5):1137-1141.

7. Teixeira MS, Swarts JD, Alper CM. Accuracy of the ETDQ-7 for identifying persons with Eustachian tube dysfunction. *Otolaryngol Head Neck Surg.* 2018;158(1):83-89.

8. Kourtidis S, Bier G, Preyer S, Hempel JM. Morphologic measurements of 3D Eustachian tube model and their diagnostic value regarding Eustachian tube dysfunction— a cross-sectional observational study. *Eur J Radiol.* 2021;136: 109563.

9. Siow JK, Tan JL. Indications for Eustachian tube dilation. *Curr Opin Otolaryngol Head Neck Surg.* 2020;28(1):31-35. doi:10.1097/MOO.0000000000000601

10. Huisman JML, Verdam FJ, Stegeman I, de Ru JA. Treatment of Eustachian tube dysfunction with balloon dilation: a systematic review. *Laryngoscope.* 2018;128(1):237-247. doi:10. 1002/lary.26800

11. Yu Y, Geffen B, McCrary H, et al. Measurements of the pediatric cartilaginous Eustachian tube: implications for balloon dilation. *Laryngoscope.* 2023;133(2):396-402. doi:10. 1002/lary.30113

12. Lien CF, Weng HH, Liu CF, Lin BS, Wu TC, Lin YS. Risk factors for internal carotid artery injury in adults during simple nasopharyngeal surgeries. *Eur Arch Otrhinolaryngol.* 2014;271(6):1693-1699. doi:10.1007/ s00405-013-2668-9

13. Abdel-Aziz T, Schröder S, Lehmann M, Gehl HB, Ebmeyer J, Sudhoff H. Computed tomography before balloon Eustachian tuboplasty—a true necessity? *Otol Neurotol.* 2014;35(4):635-638. doi:10.1097/MAO.0000000000000214

14. Bergin M, Bird P, Cowan I, Pearson JF. Exploring the critical distance and position relationships between the Eustachian tube and the internal carotid artery. *Otol Neurotol.* 2010;31(9): 1511-1515. doi:10.1097/MAO.0b013e3181f6c880

15. Haarburger C, Müller-Franzes G, Weninger L, Kuhl C, Truhn D, Merhof D. Radiomics feature reproducibility under inter-rater variability in segmentations of CT images. *Sci Rep.* 2020;10(1):12688. doi:10.1038/s41598-020-69534-6

16. Isensee F, Jaeger PF, Kohl SAA, Petersen J, Maier-Hein KH. nnU-Net: a self-configuring method for deep learning-based biomedical image segmentation. *Nat Methods.* 2021; 18(2):203-211.

17. Ding AS, Lu A, Li Z, et al. Automated registration-based temporal bone computed tomography segmentation for applications in neurotologic surgery. *Otolaryngol Head Neck Surg.* 2022;167(1):133-140.

18. Kikinis R, Pieper SD, Vosburgh K. 3D Slicer: a platform for subject-specific image analysis, visualization, and clinical support. In: Jolesz FA, ed. *Intraoperative Imaging Image-Guided Therapy.* Vol 3. Springer; 2014:277-289.

19. Dubuisson MP, Jain AK. A modified Hausdorff distance for object matching. *Proceedings of 12th International Conference on Pattern Recognition.* Vol 1. IEEE; 1994:566-568. https://ieeexplore.ieee.org/document/576361

20. Zou KH, Warfield SK, Bharatha A, et al. Statistical validation of image segmentation quality based on a spatial overlap index. *Acad Radiol.* 2004;11(2):178-189.

21. Yang F, Zamzmi G, Angara S, et al. Assessing inter-annotator agreement for medical image segmentation. *IEEE Access.* 2023;11:21300-21312. doi:10.1109/access.2023.3249759

22. Avants BB, Tustison NJ, Song G, Cook PA, Klein A, Gee JC. A reproducible evaluation of ANTs similarity metric performance in brain image registration. *Neuroimage.* 2011; 54(3):2033-2044.

23. Quammen C, Weigle C, Taylor II, RM. Boolean operations on surfaces in VTK without external libraries. *VTK J.* 2011 1-11. doi:10.54294/216g01

24. Piccinelli M, Veneziani A, Steinman DA, Remuzzi A, Antiga L. A framework for geometric analysis of vascular structures: application to cerebral aneurysms. *IEEE Trans Med Imaging.* 2009;28(8):1141-1155. doi:10.1109/TMI.2009.2021652

25. Choi SW, Lee SH, Oh SJ, Kong SK. Navigation-assisted balloon Eustachian tuboplasty for Eustachian tube dilatory dysfunction. *Clin Exp Otorhinolaryngol.* 2020;13(4):389-395. doi:10.21053/ceo.2019.01305

26. Taha AA, Hanbury A. Metrics for evaluating 3D medical image segmentation: analysis, selection, and tool. *BMC Med Imaging.* 2015;15:29.

27. Rohlfing T. Image similarity and tissue overlaps as surrogates for image registration accuracy: widely used but unreliable. *IEEE Trans Med Imaging.* 2012;31(2):153-163.

28. Ozturk K, Snyderman CH, Gardner PA, Fernandez-Miranda JC. The anatomical relationship between the Eustachian tube and petrous internal carotid artery. *Laryngoscope.* 2012;122(12): 2658-2662. doi:10.1002/lary.23679